Initial and Progressive Failure Analysis of a Composite Wing Spar Structure

Bruce Ralphin Rose.J [*1],
Priyadharshini.S [2]
Assistant Professor [1] *, PG Scholar* [2]
Department of Aeronautical Engineering,
Anna University Regional Campus, Tirunelveli, India
bruce@auttvl.ac.in [*1], *pridha92@gmail.com*[2]

ABSTRACT

In the present work, a main spar section of a composite wing structure is analyzed for its structural safety in the course of preliminary aircraft design phase. Spar is a spanwise structural member that is used to carry the bending loads and it deals with the self weight of the wing while the airplane is on the ground as well as it carries the lifting loads during flight. Because of the rolling inertia loads and chord wise bending loads caused by aerodynamic effects, spar structure is vulnerable to different structural failures before the end of safe life cycle. Initial and progressive failure analysis of the spar section is done by using the typical properties of composite materials. Carbon epoxy, Graphite epoxy and Boron epoxy materials are analyzed with their standard material properties to determine the crack initiation and propagation characteristics at different time steps with stress increments. A two-dimensional spar cross section (I - section) is designed with shell as element type and the analysis is done in ABAQUS/CAE by using XFEM for crack initiation. The results obtained through the computational analysis show the variation in crack propagation rate for different composites and it can be utilized to study the fracture mechanics in the detailed design phase of an airplane.

Keywords: *Wing spar, Composites, Initial and progressive failure, ABAQUS*

ISSN 1823- 5514, eISSN 2550-164X
Received for review: 2016-11-10
Accepted for publication: 2017-04-07
Published: 2017-12-31

Introduction

Strength and stiffness are the two major parameters of structural design that are frequently used for the manufacturing of early flight vehicles. In the recent years, the use of lighter structures for aerospace structural design is becoming a vital issue that can be achieved by means of reinforced thin walled members, multi-cell box beam configurations and semi-Monocoque constructions. The wing spar is a spanwise structural member consists of thin shear web with flange at the top and bottom of the web that is fixed normal to the fuselage to resist bending while the aircraft is on the ground. Aircraft wing composed of ribs and spars to maintain the aerodynamic shape and to yield shear loads and bending respectively. The entire weight of wing as well as the lifting loads during flight is accepted by the spar structure. Spar section carries the chordwise twisting loads, rolling inertia loads and drag forces as well caused by the aerodynamic effects. At various flight missions, all the inertial and aerodynamic forces acting on the wing structure are transmitted through the ribs to the front and rear spars [1].

Since, the spar structure carries major load components, its load bearing capacity and structural safety must be ensured to avoid unexpected failures before the safe life envelope. Typically, spar is made of aluminium alloys with tension field beams to circumvent the structural failures till the buckling limits are reached. As compared to its strength and weight, composite materials offer high strength to weight ratio with multiple advantages than the basic aluminium construction. A composite is a structural material that consists of two or more combined constituents that are combined at a macroscopic level and are not soluble in each other. For example, Graphite/ epoxy composites are approximately five times stronger than steel on a weight for-weight basis. In addition to this, the most common composites are cost effective and possess high strength with simple manufacturing process advantages.

Carbon/epoxy composites have low peak strains because the compression causes layer buckling. Some of the properties that can be improved by forming composite materials are known as strength, stiffness, corrosion resistance, wear resistance, attractiveness, weight, fatigue life, thermal insulation, and thermal conductivity [2]. Initial failure is the primary design criterion to ensure the structural safety of a composite structure [3]. Hence, the stiffness degradation phenomenon of fibre reinforced composite materials under continuous loading is an important response to predict the damage initiation [17]. The evolution of composite laminates and the corresponding damage tolerant analysis is termed as progressive failure analysis [4]. The present work is devoted to carry out the progressive failure analysis of a wing spar section through a reliable computational method.

Model Description and load calculation

A typical mid-sized airplane wing consists of front and rear spars, and it is constructed as a wing box structure. The wing box is divided into several numbers of panels and a single panel with spar section is assumed for the present failure analysis. Figure 1 shows the wing with front and rear spar sections and the wing box panel.

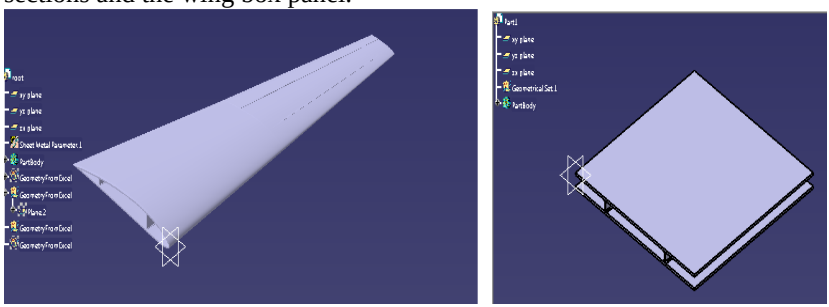

Figure 1: Wing structure and panel (wing box) with spar section

The wing structure contains two spar sections to carry the bending loads as well as to maintain its aerodynamic shape as shown in Figure 1. The required dimensions of the spar section are calculated using the airplane structural design equations for a mid-size commercial transport airplane wing [5]. Assume, the thickness of skin = 2.62 mm and a typical I-section geometry is shown in Figure 2.

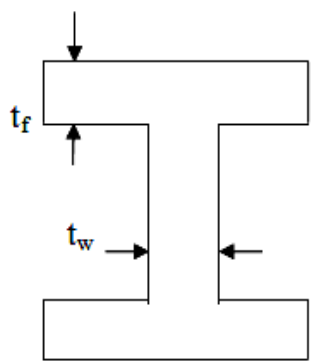

Figure 2: Typical wing spar geometry with I – section

For equal flanges, $t_f = t_w$

Thickness of the web,

$$t_w = b_w \times \frac{t_s}{b_e} \tag{1}$$

$$b_e = 2 \times b_a \tag{2}$$

$$b_w = \sqrt{\frac{b_e}{t_s}(A_{st} - 1.4 b_a t_s)} \tag{3}$$

$$t_w = b_w \times \frac{t_s}{b_e} \tag{4}$$

Loads acting on the entire wing structure are divided suitably for the selected panel with appropriate area ratio and the particular edge load is applied for the present analysis [6]. Load acting on a wing is assumed to be an Uniformly Varying Load (UVL) such that the total load is proportional to the lift profile of a wing. Maximum lift is at the airfoil root section (z =0), and for maximum lift the load factor, n = 1. The scaled takeoff gross weight of the mid-size airplane W_0 = 4800 kg and the wing span is b_w = 2.6 m. The wing structure is divided into few number of panels with each panel length = 0.6 m, hence the load acting on the whole wing must be divided in proportion to the panel [7]. Let q (z) be the lift profile of the wing, then

$$q(z) = K\sqrt{L^2 - Z^2} \tag{5}$$

$$\text{Lifting load} = \int_0^L K\sqrt{L^2 - Z^2} \tag{6}$$

$$\text{On integration, Lift} = \frac{\pi L^2 K}{4} \tag{7}$$

$$\text{In terms of load factor, } n = \frac{L}{W} \tag{8}$$

on equating,

$$\frac{W\,n}{2} = \frac{\pi L^2 K}{4} \tag{9}$$

Substituting the K value in q(z),

$$q(z) = \frac{2nW\sqrt{L^2 - Z^2}}{\pi L^2} \tag{10}$$

On substituting all values,

$$q\,(z) = 2\ \frac{K\,N}{m} \tag{11}$$

q (z) is the lift profile, therefore the lift force acting on the wing panel must be computed to initialize the failure analysis. Let us consider a panel of the wing with length 0.6 m and the load acting on the wing panel through the spar is computed as 1.2 KN.

Design and analysis tool

ABAQUS /CAE (Complete ABAQUS Environment) is a user graphical environment that is used to create the models quickly and it can be saved with different standard file formats [8] [18]. The material properties, loading conditions and boundary condition are assigned through an user friendly Graphical User Interface (GUI) module. The Finite Element Analysis (FEA) tool is preferred for the present investigation, because of the feasible analysis steps that are used to determine the progressive failure with Extended Finite Element Method (XFEM) to initiate crack growth [10]. Spar section (I-section) is also designed by using the similar CAE environment.

Wing spar design

Based on the calculated dimensions, spar section is prepared with shell element type by using ABAQUS GUI tools. The web and flange thicknesses are assumed to be equal (i.e.)., $t_w = t_f$ = 2.6 mm, and width of the flange (b_f) = 7.62 mm. The two dimensional design of spar structure made of I-section is displayed in Figure 3.

Boundary condition

In order to determine the stress - strain variations and progressive failure of the shell type spar section, a shell edge tensile load is applied at the boundary [9]. In addition, the other two edges are in the clamped condition such that the left edge of the spar is prevented from any other degree of freedom (displacement/rotation).

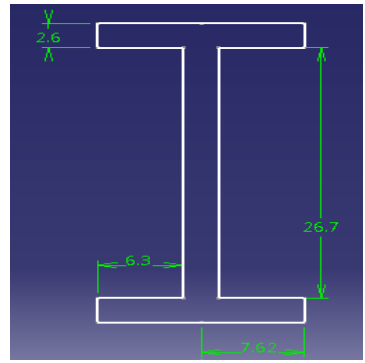

Figure 3: Wing spar design with dimensions is in *mm*

Failure Analysis

Initial and progressive failure analysis of the spar section is done by the FEA tools as a time response based investigation. The stress- strain variations at different time steps across the model is determined with crack propagation characteristics [11]. Progressive failure is termed as the crack propagation with respect to time and as the time increases crack propagates perpendicular to the load path [12]. The material properties, time step increments, necessary loads and boundary condition are applied for the spar section through the GUI. A simulation flowchart with limit failure criteria for crack initiation/propagation characteristics at different time steps with stress increments is presented in Figure 4. The minimum time step is assigned as 10 seconds and it was increased up to 100 seconds to observe the deformation scales.

The properties of carbon epoxy composite sheet are assumed as follows: Longitudinal/Transverse Young's modulus= 70 GPa, Density = 1.6 g/cm^3, In-plane shear modulus = 5 GPa, Poisson's ratio = 0.20. Similarly, for Graphite epoxy composite sheet Young's modulus = 129.4 GPa, Density = 1.51 g/cm^3, Poisson's ratio = 0.31 and for Boron epoxy Young's modulus = 420 GPa, Density = 2.45 g/cm^3, Poisson's ratio = 0.20. Loads are applied as shell edge tensile force with the prescribed edge boundary condition. Crack initiation is given by XFEM and the location of crack initiation is assigned based on the region of higher stress concentration. Free unstructured mesh type is selected for the shell elements and the model is seeded before the meshing process. Both stress and strain variations for three different materials are computed in the course of progressive failure analysis and the results are presented subsequently.

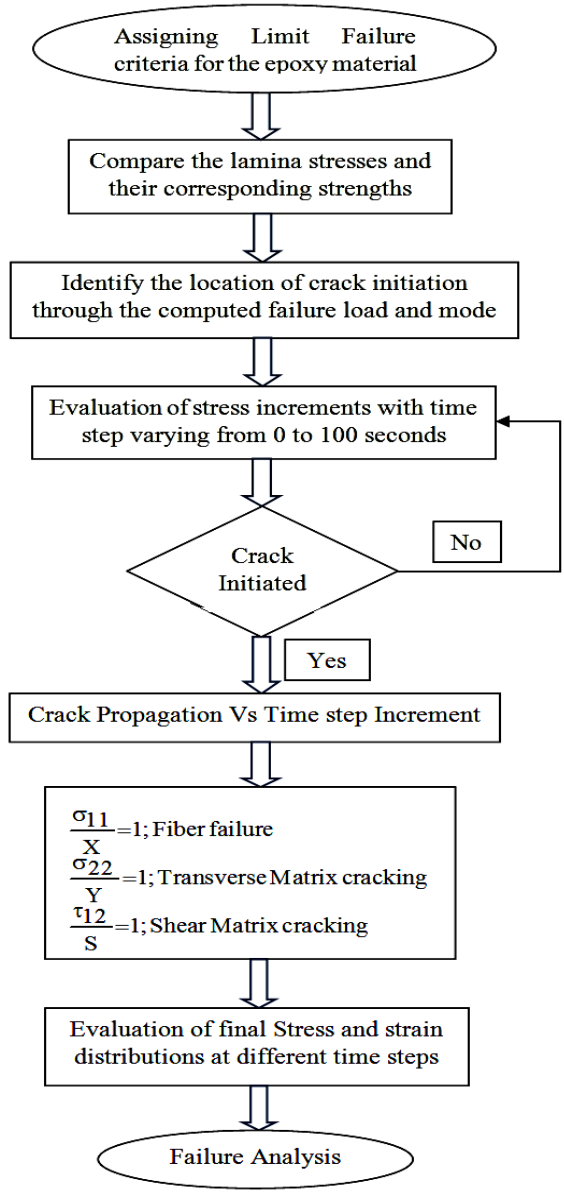

Figure 4: Simulation flowchart for the failure analysis

Crack propagation and stress-strain distribution at different time steps

Carbon epoxy

The crack initiation and propagation analysis is done as a time response FEA analysis by following the solution procedures completely using GUI. The variation of stress and strain distributions in the carbon epoxy spar at 20 seconds is highlighted in Figure 5. Maximum stress obtained at this time step is about 19.28 kPa and maximum strain corresponding to this time step is 0.153 με with the deformation scale factor = 2.944 x e^4. Crack initiates at this time step on the top flange of the section and propagates downwards (-y).

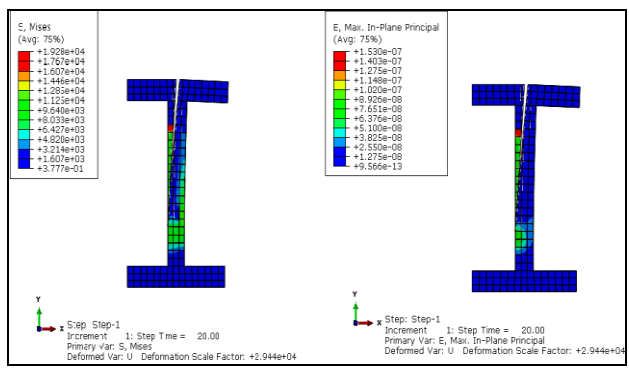

Figure 5: Stress-Strain variation in the carbon epoxy spar at 20 seconds

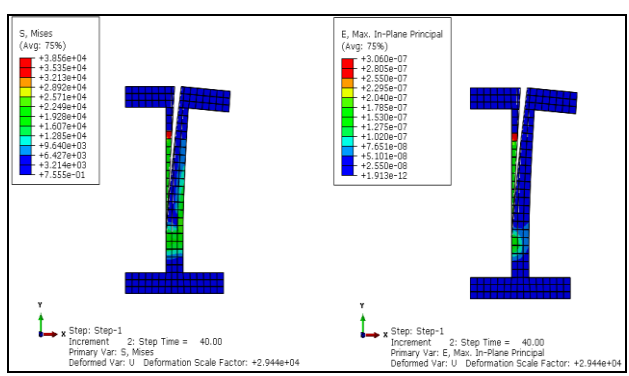

Figure 6: Stress-Strain distribution in the carbon epoxy spar at 40 seconds

The variation of stress and strain in the carbon epoxy spar at 40 seconds is presented in Figure 6. Maximum stress obtained for this time step is about 38.56 kPa and maximum strain corresponding to this time step is 0.306 με with the same deformation scale factor. Crack propagates as the time step increases from the flange to web section together with crack width and length are also increased than the previous time step. Because of the volume of the results computed, only five intermediate time steps are presented in this article.

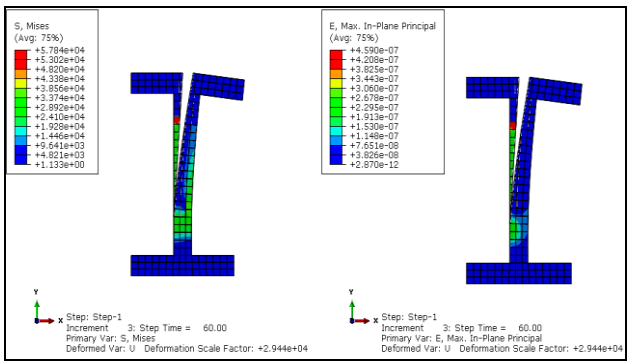

Figure 7: Stress-Strain variation in the carbon epoxy spar at 60 seconds

The variation of stress and strain in the carbon epoxy spar at 60 seconds is displayed in Figure 7. Maximum stress at this time step is 57.84 kPa and the maximum strain corresponds to this time step is 0.459 με. Crack propagates as the time step increases including the crack width and length are also increased than the previous time step. At 80 seconds, the stress magnitude increases to 77.12 kPa with strain = 0.612 με as shown in Figure 8.

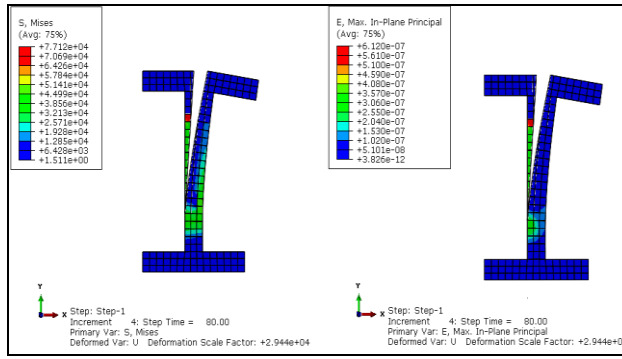

Figure 8: Stress-Strain variation in the carbon epoxy spar at 80 seconds

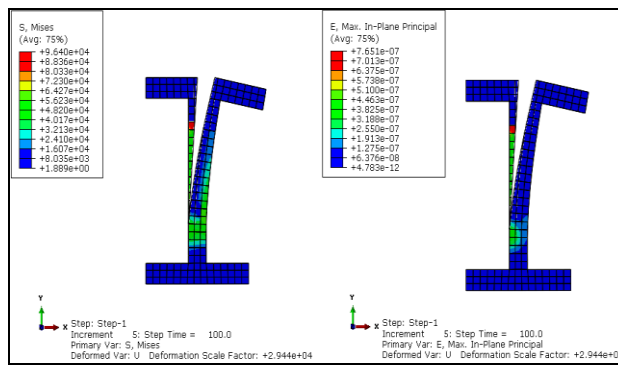

Figure 9: Stress-Strain variation in the carbon epoxy spar at 100 seconds

The variation of stress and strain in the carbon epoxy spar at the time step about 100 seconds is shown in Figure 9. Maximum stress at this time step is 96.40 kPa and maximum strain corresponds to this time step is $0.7651\,\mu\varepsilon$. Crack width and length are increased than the previous time step and this is the final stage of failure because it has reached the ultimate limit. A significant redistribution of stresses is observed in the web portion of the spar because of the progressive failure occurred.

Graphite epoxy

The primary stress-strain variations in the graphite epoxy spar are indicated through three different time steps at 20, 60, and 100 seconds respectively. The maximum stress (σ_{max}) at 20 seconds step is about 19.15 kPa and

maximum strain (ε_{max}) corresponds to this time step is 0.1.473 $\mu\varepsilon$ with deformation factor is 3.038 x e^4. Crack initiates at this step at the mid portion of the top flange in the I-section and propagates as time increases as illustrated in Figure 10.

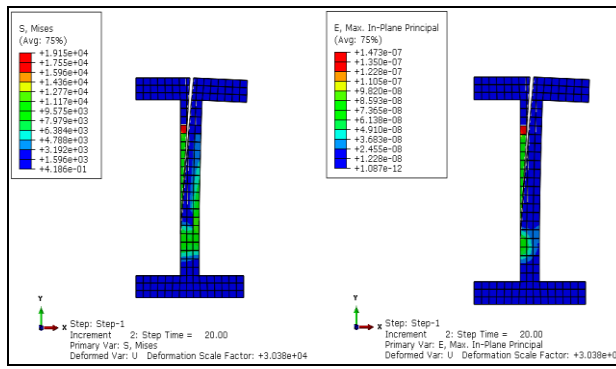

Figure 10: Stress-Strain variations in the graphite epoxy spar at 20 seconds

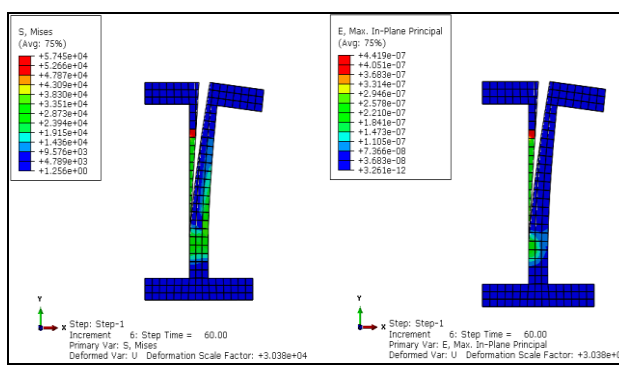

Figure 11: Stress-Strain variations in the graphite epoxy spar at 60 seconds

The variation of stress and strain of graphite epoxy spar at 40 seconds is computed with σ_{max} = 38.30 kPa and ε_{max} = 0.2946 $\mu\varepsilon$. In the same fashion, The stress and strain distribution in the graphite epoxy spar at 60 seconds is shown in Figure 11. σ_{max} at this time step is about 57.45 kPa, with ε_{max} = 0.4419. Crack propagates towards the negative y-direction as the

time increases, crack width and length are also increased than the previous time steps.

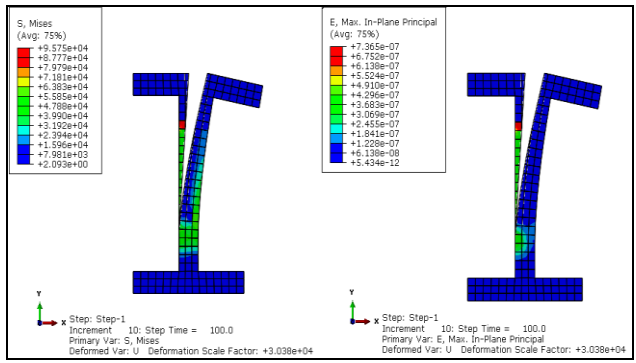

Figure 12: Stress-Strain variation in the graphite epoxy spar at 100 seconds

The variation of stress and strain in the graphite epoxy spar at 80 seconds is computed as σ_{max} = 76.6 kPa and maximum strain corresponds to this time step is 0.5892 $\mu\varepsilon$. The stress and strain distribution in the graphite epoxy spar at 100 seconds is shown in Figure 12. At this time step, σ_{max} = 95.75 kPa and ε_{max} = 0.7.365 $\mu\varepsilon$. Crack propagates linearly as the time step increases, and its width and length are also increased till the final stage of structural failure.

Boron epoxy

Boron epoxy composites are superior than glass-reinforced composites to structures where stiffness is a primary design consideration. Recently, NASA Langley Research Center (LRC) investigated the potential of boron filament to use it for aerospace vehicle structures. The primary stress-strain distributions in the boron epoxy spar at three intermediate time steps are presented at this point similar to the previous case. The maximum stress at 20 seconds is about σ_{max} = 18.98 kPa, and ε_{max} = 0.09731 $\mu\varepsilon$ as shown in Figure 13. Deformation factor is 4.559 x e^4. Crack is initiated at the mid-portion of the top flange in the I-section and it propagates as the time step increases similar to the graphite epoxy material.

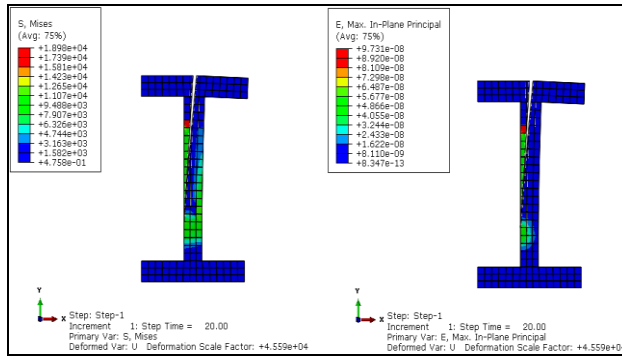

Figure 13: Stress-Strain distribution in the boron epoxy spar at 20 seconds

The computed σ_{max} value at 40 seconds for the boron epoxy spar is about 37.95 kPa and ε_{max} = 0.1946 $\mu\varepsilon$. The stress and strain distributions in the boron epoxy spar at 60 seconds are shown in Figure 14. σ_{max} at this time step is 56.93 kPa, and ε_{max} = 0.2919 $\mu\varepsilon$. Crack propagates as the time step increases because of the reduced stiffness in the progressive failure simulation.

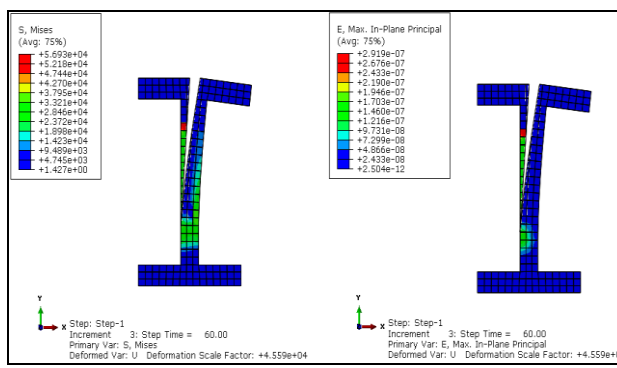

Figure 14: Stress-Strain variation in the boron epoxy spar at 60 seconds

The maximum stress and strain in the boron epoxy spar at 80 seconds is about σ_{max} = 75.90 kPa, and ε_{max} = 0.3892 $\mu\varepsilon$. Similarly, the variation of stress and strain of boron epoxy spar at 100 seconds is shown in Figure 15. Maximum stress at this time step is σ_{max} = 94.88 kPa and maximum strain

corresponds to this time step is $\varepsilon_{max} = 0.4866\ \mu\varepsilon$. Crack width and length are increased than the previous time step and this failure mode reveals the characteristics of damage mechanics through coupled FEA analysis.

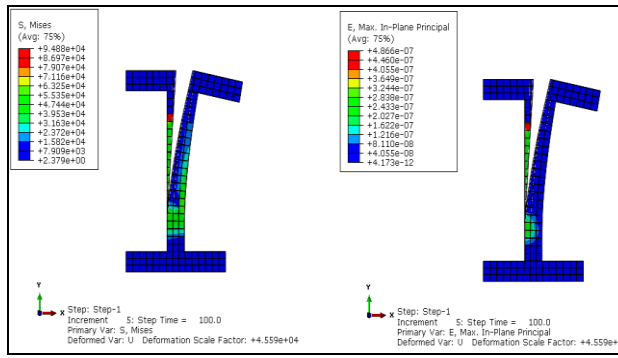

Figure 15: Stress-Strain variation in the boron epoxy spar at 100 seconds

Results and Discussion

Stress-strain curve at various time steps

In the course of structural design of airplane components, the failure stress-strain analysis plays an important role. Figure 16 presents the computed maximum stress strain variations of three different materials at 10 successive time step intervals. From the results, it is observed that the stress variations exist in the carbon and graphite epoxy spars is close to each other. Boron epoxy has stress and strain values that are less compared to the other two epoxy composite spars. The distribution of stress with respect to time at different spanwise locations is also observed through the 3D simulations to ensure the Factor of Safety (FoS) of the proposed material [19]. Stress increases linearly as time increases. Crack propagates as the time step increases together with the incremental in-plane stresses that are assigned by the number of the sub steps in the progressive failure simulations. The micro scaled crack initiates at 20 seconds and propagates as time increases with increasing stress values, and the final failure occur at maximum stress about 96.4 kPa.

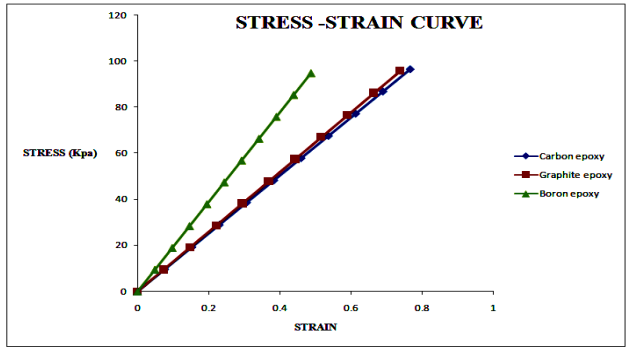

Figure 16:Stress-strain curves for carbon, graphite and boron epoxy materials

From the computed failure stress and strain values for graphite epoxy material at different time step starting from 20 seconds to 100 seconds, it is interestingly realized that as the crack propagation is rapid after 50 seconds because of the fully weakened elements [20]. Similarly, for boron epoxy material at different time steps starting from 20 seconds to 100 seconds, the crack and propagation is severe after 70 seconds because of the inherent stress hardening abilities. The linear variation of stress values with respect to time is computed and the final failure occurs at maximum stress about 94.88 kPa and the corresponding strain is 0.4866 $\mu\varepsilon$.

Conclusions

Based on the results presented in the article, it is concluded that with the simplified methods, preliminary sizing of the wing structures can be performed with enough confidence. The results show that the stress strain magnitudes of carbon and graphite epoxy materials are close to each other and their crack propagation rate is also exhibiting the similar behaviour. Meanwhile, the stress-strain values for boron epoxy spar are comparatively less than the other two materials.

The characteristic of progressive failure rate is studied in this investigation through the crack initiation process to the final failure mode. Finally, initial and propagation of crack at spar (I-section) for the three composite materials have been evaluated. Results of the simplified method of analysis shows that the algorithm is applicable for performing the preliminary sizing of the wing structure before moving on to the more refined finite element based coupled failure analysis. Further, the failure characteristics of epoxy spars at different loading conditions (impact, fatigue,

etc) other than in- plane shear loads can be done using this progressive failure investigation with optimum accuracy and less computing time.

References

[1] Autar K.Kaw, Mechanics of composite materials second edition ISBN 0-8493-1343-0 (2006).

[2] Robert M.Jones,Mechanics of composite materials second edition ISBN 1-50632-712-X (1999).

[3] Kim JH and Lee CS, Initial and progressive failure analyses for composite laminates using puck failure criterion and damage-coupled finite element method. Composite Structures 121- 406–419 (2014).

[4] Jabir Ubaid, Strength prediction and progressive failure analysis of carbon fiber reinforced polymer laminate with multiple interacting holes involving three dimensional finite element analysis and digital image correlation. International Journal of Damage Mechanics, Vol. 23(5) 609–635(2013).

[5] Sridhar Chintapalli, Preliminary structural design optimization of an aircraft wing box ISBN 978-0-494-20758-1 (2006).

[6] Chung MS and Lee CS, Numerical evaluation for debonding failure phenomenon of adhesively bonded joints at cryogenic temperature. Composites Science and Technology 71-1921–1929 (2011).

[7] Hinton MJ and Soden PD, A comparison of the predictive capabilities of current failure theories for composite laminates. Composites Science and Technology 62 -1725–1797 (1998).

[8] Kim SK and Lee CS, Computational evaluation of resistance of fracture capacity for SUS304L of liquefied natural gas insulation system under cryogenic temperatures using ABAQUS user-defined material subroutine. Materials and Design, 50-522–532(2013).

[9] Kaddour AS, A comparison of the predictive capabilities of current failure theories for composite laminates: additional contributors. Composites Science and Technology 64 -449–476(2003).

[10] Kim JM and CS Lee, Prestrain-dependent viscoplastic damage model for austenitic stainless steel and implementation to ABAQUS user-defined material subroutine. Computational Materials Science 67 -273–281 (2012).

[11] JM Lee and CS Lee, Failure analysis of reinforced polyurethane foam-based LNG insulation structure using damage-coupled finite element analysis. Composite Structures 107 -231–245 (2013).

[12] Liu PF, Progressive failure analysis of carbon fiber/epoxy composite laminates using continuum damage mechanics. Materials Science and Engineering A 485 -711–717 (2008).

[13] Maimi camanho P, A continuum damage model for composite laminates: Part I – Constitutive model. Mechanics of Materials 39 - 897–908 (2006).
[14] Maimi P and Mayugo JA, A Three-dimensional Damage Model for Transversely Isotropic Composite Laminates. Journal of composite materials, Vol. 42, No. 25 (2008).
[15] Puck A, Failure analysis of FRP laminates by means of physically based phenomenological models. Composites Science and Technology 58-1045±1067 (1996).
[16] Toi.Y, Thermal Elasto-Viscoplastic Damage Behavior of Structural Members in Hot-Dip Galvanization. International Journal of damage mechanics, Vol. 11, 1056-7895/02/02 0171–15 (2002).
[17] Kevin Hoos, Endel V. Iarve , Progressive Failure Simulation in Laminated Composites under fatigue loading by using discrete damage modeling AIAA 2016-0726 (2016).
[18] M. V. Kozlov and S. V. Sheshenin Modeling the progressive failure of laminated composites. DOI 10.1007/s11029-016-9540-0 (2016).
[19] S. P. Engelstad, J.E. Action, S.B. Clay, R.C. Holzwarth, D. Robbins, "Assessment of Composite Damage Growth Tools for Aircraft Structure, Part I," Proceedings of the AIAA SciTech 2015 Conference, Orlando, FL, Jan 2015.
[20] Iarve, E.V., Gurvich, M.R., Mollenhauer, D.H., Rose, A.C. and Davila, C.G. Mesh-independent matrix cracking and delamination modeling in laminated composites, Int. J. Numerical Methods in Engineering, 88(8), pp. 749-773, 2011.